Molecular Therapy
Nucleic Acids
Original Article

Inefficacy of anti-VEGF therapy reflected in VEGF-mediated photoreceptor degeneration

Xin Xu,[1] Ni Han,[1] Fangkun Zhao,[4] Ruoyue Fan,[3] Qingguo Guo,[1,2] Xuefei Han,[3] Ying Liu,[2] and Guangzuo Luo[1,3]

[1]Institute of Health Sciences, China Medical University, Shenyang 110122, China; [2]Department of Biochemistry and Molecular Biology, China Medical University, Shenyang 110122, China; [3]Bionce Biotechnology, Co., Ltd, Nanjing 210061, China; [4]Department of Ophthalmology, The Fourth Affiliated Hospital of China Medical University, Shenyang 110005, China

Retinal neovascularization (RNV) is primarily driven by vascular endothelial growth factor (VEGF). However, current anti-VEGF therapies are limited by short half-lives and repeated injections, which reduce patient quality of life and increase medical risks. Additionally, not all patients benefit from anti-VEGF monotherapy, and some problems, such as unsatisfactory vision recovery, persist after long-term treatment. In this study, we constructed a recombinant adeno-associated virus (AAV), AAV2-SPLTH, which encodes an anti-VEGF antibody similar to bevacizumab, and assessed its effects in a doxycycline-induced *Tet-opsin-VEGFA* mouse model of RNV. AAV2-SPLTH effectively inhibited retinal leakage, RNV progression, and photoreceptor apoptosis in a *Tet-opsin-VEGF* mouse model. However, proteomic sequencing showed that AAV2-SPLTH failed to rescue the expression of phototransduction-related genes, which corresponded to reduced photoreceptor cell numbers. This study suggests that anti-VEGF monotherapy can significantly inhibit RNV to some extent but may not be enough to save visual function in the long term.

INTRODUCTION

Many retinal diseases, such as age-related macular degeneration (AMD), diabetic retinopathy, and retinopathy of prematurity, are characterized by retinal neovascularization (RNV).[1–3] RNV can cause vitreous hemorrhage, retinal detachment, inflammation, tissue edema, and fibrotic scar formation, among other pathological changes, ultimately causing irreversible vision loss and blindness.[4–6]

Vascular endothelial growth factor (VEGF) is considered the main driver of RNV, for which a major treatment is anti-VEGF therapy using ranibizumab, bevacizumab, aflibercept, or brolucizumab.[4] However, there are two main limitations to current anti-VEGF therapies. Bevacizumab, ranibizumab, and aflibercept are expensive and require repeated intraocular injections.[7] The short half-life of existing anti-VEGF therapies exacerbates the economic burden on patients and increases the medical risks.[8] Many patients also suffer from recurrence or worsening of RNV-associated disease activity following an initial positive anatomical and visual response despite the continuation of anti-VEGF therapy. A randomized controlled trial reported a 40.7% incidence of subretinal fibrosis after anti-VEGF therapy in patients with RNV.[9] Eng et al. found that aflibercept, bevacizumab, and ranibizumab treatments caused comparable degrees of outer retinal atrophy in patients with AMD at 24 months.[10] The incomplete therapeutic efficiency of anti-VEGF treatments emphasizes the need for further elucidating the mechanisms and therapeutic targets of RNV to develop new and effective treatment strategies.

The adeno-associated virus (AAV) is an efficient and safe retinal gene delivery vehicle that can prevent or arrest disease progression for a lasting treatment.[11–13] Successful gene supply in RNV-associated diseases, such as RGX-314, ADVM-022, or 4D-150, may exert long-lasting disease control in the general population.[14–17]

To overcome the current limitations of anti-VEGF treatments in RNV, we constructed and validated the therapeutic effects of a novel recombinant AAV, AAV2-SPLTH. Similar to bevacizumab, AAV2-SPLTH was designed to promote the long-term expression of anti-VEGF antibodies *in vivo* and *in vitro*. In a *Tet-opsin-VEGFA* mouse model, we examined the long-term efficacy of AAV2-SPLTH on RNV using fundus fluorescein angiography (FFA) and hematoxylin and eosin (H&E) staining. Furthermore, we examined the potential mechanisms of RNV and the insufficient therapeutic effect of AAV2-SPLTH using proteotranscriptome analysis. This study elucidates the pathogenesis of RNV and provides a potential strategy for combined treatments of RNV-related diseases.

RESULTS

Construction and *in vitro* testing of AAV2-SPLTH

AAV2-SPLTH uses an AAV serotype 2 (AAV2) capsid as a vector to deliver and encode bevacizumab, an anti-VEGF monoclonal antibody, the sequence of which is from DrugBank (https://go.drugbank.com/). A schematic representation of the AAV2-SPLTH genome is shown in Figure 1A. Anti-VEGF cDNA was inserted into an expression cassette containing the chiken beta-actin (CBA) promoter, which

Received 31 October 2023; accepted 19 March 2024;
https://doi.org/10.1016/j.omtn.2024.102176.

Correspondence: Ying Liu, Department of Biochemistry and Molecular Biology, China Medical University, Shenyang 110122, China.
E-mail: liuying@cmu.edu.cn
Correspondence: Guangzuo Luo, Institute of Health Sciences, China Medical University, Shenyang 110122, China.
E-mail: gzluo@cmu.edu.cn

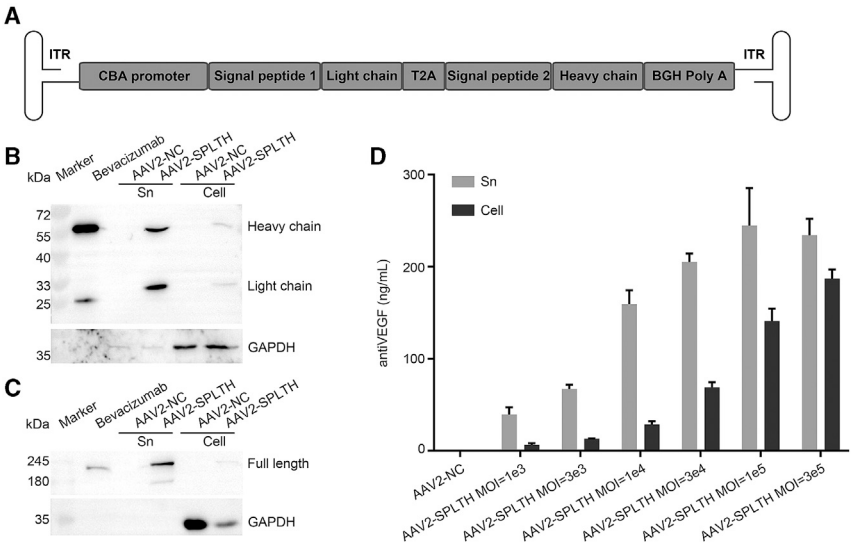

Figure 1. Construction and *in vitro* testing of AAV2-SPLTH

(A) Schematic representation of AAV2-SPLTH vector. ITR, inverted terminal repeat of AAV2; CBA, chicken beta-actin promoter; T2A, Thosea asigna virus 2A self-cleaving peptide; BGH poly(A), bovine growth hormone polyadenylation signal. (B) Antigen specificity of heavy-chain and light-chain antibodies secreted by AAV2-SPLTH under reducing conditions. (C) Antigen specificity of IgG1 antibodies secreted by AAV2-SPLTH under non-reducing conditions. (D) The anti-VEGF secreted in the supernatants was determined using ELISA. Data are presented as mean ± SD (n = 3).

drives VEGF expression. The light-chain and heavy-chain sequences of bevacizumab are separated by a Thosea asigna virus 2A self-cleavage site. Signal peptides 1 and 2 were designed to enhance the expression of the light and heavy chains, respectively.

To validate the successful assembly, we performed western blotting to detect the expression of anti-VEGF antibodies secreted by infected HEK293T cells. The HEK293T cells were infected with AAV2-SPLTH or AAV2-NC (negative control); bevacizumab was used as a positive control. In the infected cells and cell supernatants of the AAV2-SPLTH group, dissociation into heavy (55 kDa) and light (25 kDa) chains was observed under reducing conditions (Figure 1B). The expected single 180 kDa band of the immunoglobulin G1 (IgG1) antibody was observed under non-reducing conditions (Figure 1C). VEGF-binding activity was observed in infected cells and cell supernatants by enzyme-linked immunosorbent assay (ELISA) and was enhanced with increased MOI of AAV2-SPLTH (Figure 1D).

Anti-VEGF effect of AAV2-SPLTH *in vitro*

To verify the anti-VEGF effect of AAV2-SPLTH *in vitro*, we performed VEGF-dependent cell proliferation, migration, and tube formation assays using human umbilical vein endothelial cells (HUVECs). As shown in Figure 2, 50 ng/mL VEGF significantly promoted cell proliferation, migration, and tube formation, whereas 200 ng/mL bevacizumab had a remarkable inhibitory effect. Compared to VEGF, AAV2-SPLTH inhibited HUVEC proliferation, migration, and tube formation, which is similar to bevacizumab, supporting the anti-VEGF effect of AAV2-SPLTH *in vitro*.

AAV2-SPLTH improves vascular pathologies in the *Tet-opsin-VEGFA* mouse model

RNV-associated retinal diseases often show adverse alterations in ocular vessels, such as vascular leakage.[18–20] To assess the efficacy of AAV2-SPLTH *in vivo*, we first evaluated its effect on vascular leakage in a *Tet-opsin-VEGFA* mouse model. *Tet-opsin-VEGF* double-transgenic mice, in which the Tet-On system and rhodopsin promoter provide doxycycline-inducible expression of $VEGF_{165}$, develop exudative retinal detachment within 4 days of receiving 2 mg/mL doxycycline in their drinking water.[21] In our study, *Tet-opsin-VEGFA* double-transgenic mice received 2 mg/mL doxycycline through their drinking water after 2 weeks of intravitreal injection with 2 μL AAV2-NC or intravitreal monocular injection with 3×10^9 Genomic Copies (GC) AAV2-SPLTH. FFA showed that increased vascular leakage was induced 10 days after doxycycline induction in *Tet-opsin-VEGFA* mice, as manifested by a strong fluorescence signal outside the blood vessels (Figure 3A, white circle). At 30 days after doxycycline induction, vascular leakage increased, and severe retinal detachment occurred (Figure 3A, white arrow). At 10 or 30 days after induction, intravitreal injection of AAV2-SPLTH significantly inhibited vascular leakage, unlike the effects of AAV2-NC, as demonstrated by a significant reduction in the size and number of extravascular fluorescein regions (Figure 3B).

RNV is also accompanied by pathological angiogenesis and edema resulting in increased retinal thickness or even retinal detachment, ultimately leading to irreversible blindness.[5,20] In contrast to the increased retinal thickness and detached retinas in the control or AAV2-NC group, H&E staining suggested that AAV2-SPLTH improved the retinal structure in *Tet-opsin-VEGFA* mice both at 10 and 30 days after doxycycline induction (Figure 3B). Notably, photoreceptor cell numbers in the retinas of the AAV2-SPLTH group decreased 30 days after induction, indicating that treatment with AAV2-SPLTH could not prevent photoreceptor cell death in *Tet-opsin-VEGFA* mice (Figures 3C and 3D). We performed TUNEL staining to examine changes in apoptosis in the retinas of *Tet-opsin-VEGFA* mice and found that compared to the control or AAV2-NC group, the AAV2-SPLTH group showed significantly decreased levels of apoptosis 10 days after induction (Figure 4A). However, the levels of apoptosis increased in the retinas after 30 days; thus, AAV2-SPLTH failed over longer-term treatment (Figure 4B).

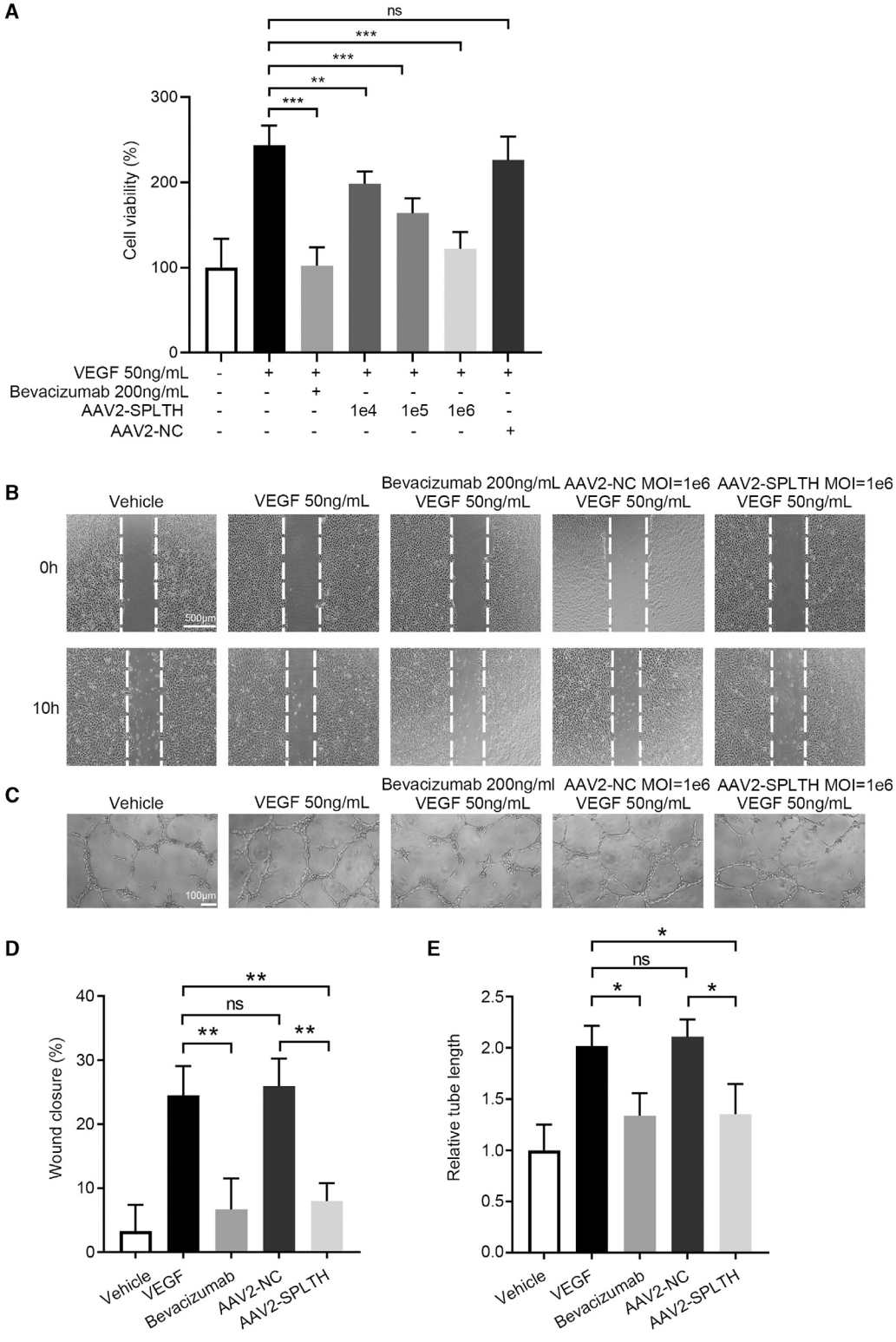

(legend on next page)

Proteomic analysis of retinas treated with AAV2-SPLTH

To identify the core genes, biological processes, and signaling pathways involved in the onset of RNV and efficacy of the AAV2-SPLTH treatment, we performed proteomic analyses of proteins extracted from the retinas of *Tet-opsin-VEGFA* mice without doxycycline induction (NC), *Tet-opsin-VEGFA* mice with doxycycline induction (control), and mice treated with AAV2-SPLTH. The data were stratified according to groups, and the corresponding net values were compared.

As shown in Figures 5A and 5B, compared with protein expression in the control group, a total of 305 proteins were detected to have increased expression and 533 proteins to have decreased expression in the NC group and 265 proteins to have increased expression and 535 proteins to have decreased expression in the AAV2-SPLTH group. There were a total of 288 different proteins with consistent changes, such as chitinase-like protein 3 (Chil3), calcareous protein S100-A9 (S100A9), and neutrophil gelatinase-associated lipocalin (LCN2), which may be the key molecules directly involved in VEGF induction of fundus vascular lesions in *Tet-opsin-VEGFA* mice, defined as intersection I (rescue differential protein collection). There were 550 different proteins with inconsistent changes, such as Recoverin (Rcvrn) and other molecules, which may be secondary changes in fundus vascular lesions in *Tet-opsin-VEGFA* mice mediated by VEGF, defined as intersection II (unsaved differential protein set). The above intersection results are shown in Figure 5C's UpSet Venn diagram. We performed Kyoto Encyclopedia of Genes and Genomes (KEGG) enrichment analysis to identify the biological processes and signaling pathways associated with the curative and uncured DEPs. Both curative and uncured different expressed proteins (DEPs) were involved in the phototransduction signaling pathway, implying that AAV2-SPLTH treatment is inadequate for complete photoreceptor rescue (Figures 5D and 5E). In order to verify the reliability of protein sequencing data, 10 indexes with the most significant differential expression changes were selected for qPCR validation. The expression of these genes was consistent with the sequencing results, supporting the reliability of the sequencing data (Figure S1). Furthermore, in view of the important role of phototransduction signaling pathways in visual function, differential proteins enriched by phototransduction signaling pathways were selected for preliminary qPCR verification at the mRNA level. As shown in Figure S2A, in control group, the mRNA expression of rhodopsin (Rho) was the most significantly downregulated, and in the AAV2-anti-VEGF group, it basically recovered to the same level as that in the NC group. The expression of cyclic nucleotide-gated cation channel alpha-1 (Cnga1) and guanylyl cyclase-activating protein 1 (Gcap1), and guanylate cyclase activator 1A (Guca1a) was decreased in the control group and restored to the same expression level in the NC group as in the AAV2-anti-VEGF group. As shown in Figure S2B, compared with the NC group, rod cGMP-specific 3′,5′-cyclic phosphodiesterase subunit beta was significantly decreased in the control group, and Pde6b and guanine nucleotide-binding protein G(I)/G(S)/G(T) subunit beta-1 (Gnb1) were significantly decreased in the AAV2-anti-VEGF group. The above results were consistent with those of proteomic detection.

AAV2-SPLTH failed to rescue photoreceptor degeneration in the *Tet-opsin-VEGFA* mouse model

Further analysis of phototransduction signaling pathways involving uncured proteins showed that RCVRN was the most significant DEP. Rho was the most significant DEP in the phototransduction signaling pathways involving curative proteins. To compare the differences in the distribution of Rho and RCVRN, we performed immunofluorescence on the retinas of *Tet-opsin-VEGFA* mice 10 days after induction. Consistent with previous reports, Rho was mainly distributed in rod photoreceptor cells, for which it is a known marker (Figure 6B).[22] Compared to Rho, RCVRN was distributed across the photoreceptor cell layer (Figure 6A). Compared to the control group, which showed few fluorescence signals for Rho, the AAV2-SPLTH group showed a significant increase in the fluorescence intensity of Rho, indicating that AAV2-SPLTH maintained Rho expression. However, there was no significant difference in the fluorescence intensity of RCVRN between the control and AAV2-SPLTH groups, indicating that AAV2-SPLTH failed to rescue the expression of RCVRN. Similar results were observed using western blotting, proving the differential therapeutic effects of AAV2-SPLTH on Rho and RCVRN (Figures 7A–7D). In addition, electroretinogram (ERG) analysis showed a remarkable recovery effect of sight in the AAV2-SPLTH group 10 days after induction and an impaired effect 30 days after induction (Figures 7E and 7F).

DISCUSSION

This study describes a novel recombinant AAV2-SPLTH-based gene therapy that can maintain long-term secretion of anti-VEGF antibodies, similar to bevacizumab. Since the off-label use of bevacizumab in the treatment of wet AMD achieved promising results in 2005 and ranibizumab was approved for the treatment of AMD in 2006, an increasing amount of anti-VEGF drugs have entered the pre-clinical and developmental stages.[23] Bevacizumab is the first monoclonal antibody with a molecular weight of 149 kDa to effectively inhibit VEGF targets and the first drug used against neovascular AMD.[24] Studies have shown that ranibizumab is more permeable than bevacizumab through the highly polarized RPE layer at clinically equivalent concentrations.[25] Although ranibizumab has the advantages of small molecular weight and strong penetration, in clinical trials, there

Figure 2. AAV2-SPLTH inhibits proliferation, migration, and tube formation of HUVECs

(A) The results of cell proliferation assay of HUVECs after different treatments. Data are presented as mean ± SD ($n = 3$). (B) The binary image results of wound-healing assays using HUVECs at 0 and 10 h after different treatments. Scale bars: 500 μm. (C) The results of tube formations of HUVECs after different treatments. Scale bars: 100 μm. (D) Analysis of the wound-healing area rates at 10 h. Data are presented as mean ± SD ($n = 3$). (E) Analysis of the tube lengths. Data are presented as mean ± SD ($n = 3$). One-way ANOVA method was applied for statistical analysis $^{*}p < 0.05$, $^{**}p < 0.01$, $^{***}p < 0.001$, $^{****}p < 0.0001$, ns, not significant.

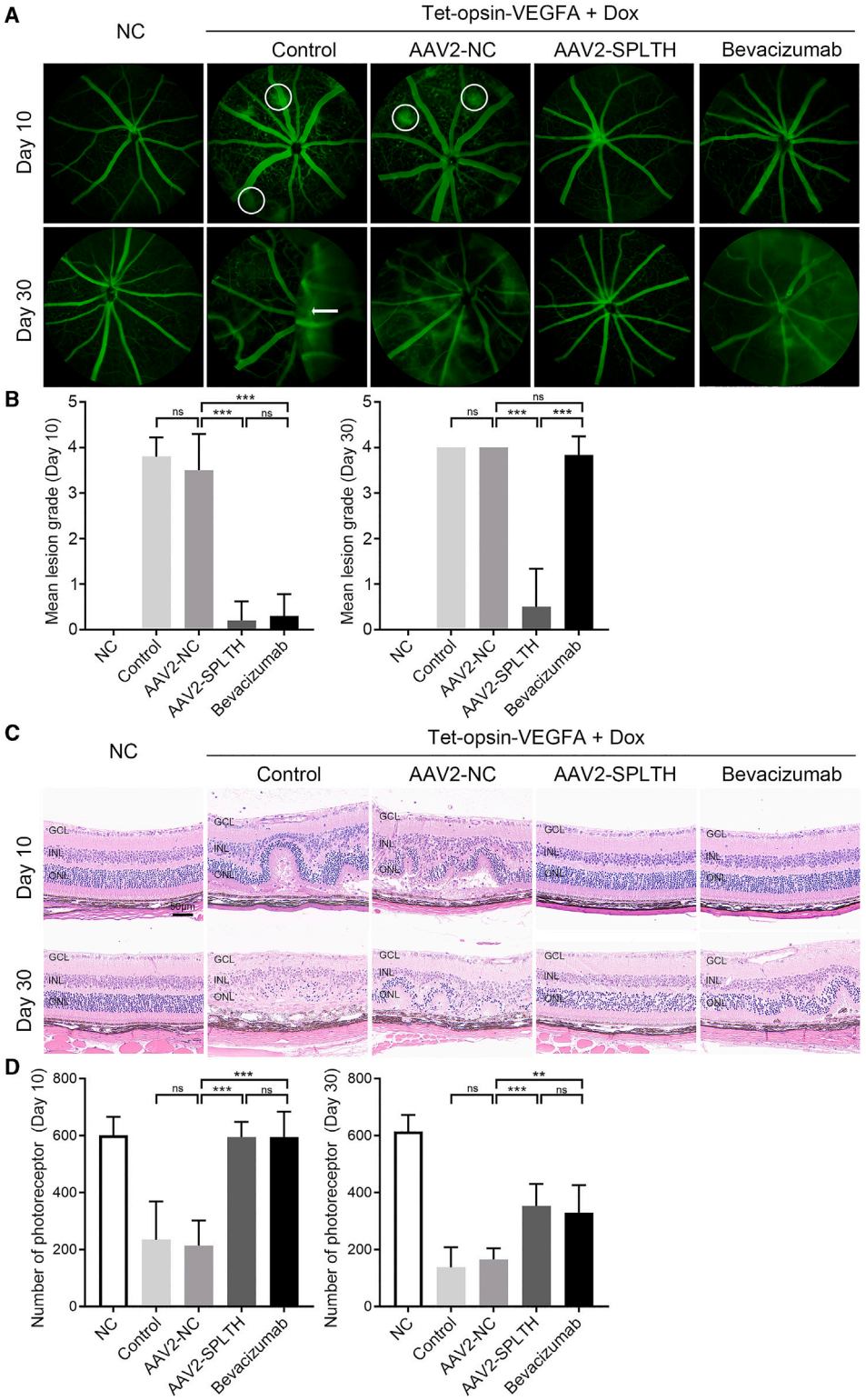

(legend on next page)

was no apparent differences in the efficacy of intravitreal injections of bevacizumab, ranibizumab, and aflibercept in the treatment of diabetic macular oedema (DME) and AMD, especially when baseline vision was slightly reduced.[26–28] In theory, Fc fragments can bind to Fc receptors and easily enter systemic circulation through active transport to increase systemic adverse events. However, a number of clinical studies have shown that Fc fragments cannot easily mediate the transport of drugs across the blood-retina barrier, and anti-VEGF drugs containing Fc fragments do not increase the risk of systemic adverse events.[29] In addition, in the human eye, the aqueous half-life of intravitreally injected bevacizumab is 9.82 days, while for ranibizumab and aflibercept, the half-lives are 9.19 and 11.4 days, respectively.[30–32] Because of the short half-life, frequent injections of antibody drugs are required to maintain efficacy. This not only increases medical risks but also creates a huge financial burden for patients. Gene therapy can avoid this problem by achieving long-term sustained expression with a single injection.[33] Currently, there are clinical trials of the gene therapy drugs aflibercept and ranibizumab delivered via AAV vector, which have shown good therapeutic effect on fundus angiogenesis disease.[14,24] The studies suggests the effectiveness of AAV delivery of anti-VEGF strategies. Studies on AAV delivery of different forms of anti-VEGF antibodies will provide new drug options for fundus angiogenesis diseases. Therefore, we explored the effect of AAV delivery of anti-VEGF similar to bevacizumab in fundus angiogenesis diseases.

Choosing the right serotype is critical for both the safety and effectiveness of AAV-mediated gene therapy.[34] Studies have shown that intravitreal injection of AAV2, -8, and -9 can infect ganglion cells of the internal limiting membrane at the retinal junction; however, glass restricts the transduction of AAV8 and -9 to the cells inside the retina. Only AAV2 can effectively be transduced into retinal cells after intravitreal injection.[35] AAV2 was the first successful carrier used for commercial retinal gene therapy drugs: in 2017, the US Food and Drug Administration approved Luxturna for the treatment of hereditary vision loss caused by the RPE65 gene mutation, which was delivered to retinal cells via the AAV2 vector to treat Leber congenital amaurosis type 2.[36] These studies suggest that AAV2 vectors are an effective and safe option for gene therapy in eye diseases.

To better evaluate the effect of VEGF antibody drugs in animals, we used CRISPR-Cas9 technology to construct humanized *Tet-opsin-VEGFA* mice and realized an animal model that can specifically express human VEGF through doxycycline stimulation of retinal photoreceptor cells and show a long-term stable fundus angiogenesis phenotype. In this model, 6- to 8-week-old *Tet-opsin-VEGFA* mice were used, and the mRNA and protein levels of $VEGF_{165}$ were significantly increased in doxycycline-induced conditions compared to those in the control group, while the expression of $VEGF_{165}$ showed little change, reflecting that the TIGRE site can achieve the lowest basal expression of the inserted gene and high induction activity.[37] Compared to the traditional Rho-VEGF randomly targeted transgenic mouse model, there are two main advantages. First, animal genome information is clearer, making experiments on different animal models more repeatable. Second, Tet-On technology can control the timing of the fundus angiogenesis phenotype in mice through doxycycline administration, which solves the bottleneck of the fundus angiogenesis phenotype appearing in mice with sustained VEGF expression at 2–3 weeks of age.[38] The commonly used fundus angiogenesis models mainly include oxygen-induced retinopathy mouse models and laser-induced choroidal angiogenesis rat and monkey models. Although existing models can simulate the fundus angiogenesis phenotype, they are limited by a short experimental window and self-healing of lesions, which are not conducive to the long-term observation of disease progression and evaluation of drug efficacy. In addition, current mouse models are established with the increased expression of murine-derived VEGF, which is not suitable for the validation of humanized VEGF antibody effects. Therefore, humanized *Tet-opsin-VEGFA* mice provide a reliable experimental model for pre-clinical efficacy evaluation. In addition, the intraocular radius of small animals is small, and the intraocular distribution varies greatly between species.[28,39] In subsequent further studies, the experimental development of laser-induced choroidal angiogenesis model in non-human primates will help to fully verify the effect of the drug, and the model does not have species-specific problems.[40]

Although intravitreal injection of anti-VEGF agents has been recommended as a first-line treatment for fundus angiogenesis disease, a sizable population of patients do not respond to anti-VEGF therapies.[41] Approximately 25%–30% of patients with AMD show refractory responses in the early stages of anti-VEGF treatment.[42] These patients usually present with persistent (plasma) fluid exudation, unresolved or new hemorrhage, progressive lesion fibrosis, and/or suboptimal vision recovery.[4] Except for the refractory complications described above, long-term anti-VEGF monotherapy resulted in photoreceptor deregulation or even apoptosis in the retinas of mice with RNV.[43,44] Therefore, understanding disease pathogenesis is particularly important for optimizing diagnostic and treatment strategies and developing multi-target combination therapies. In this study, we found that long-term doxycycline administration caused vascular-related pathological changes in *Tet-opsin-VEGFA* mice along with a significant reduction in the number of photoreceptor cells. However, the AAV2-SPLTH group showed no vascular-related pathological changes, only a decrease in the number of photoreceptor cells consistent with reports that photoreceptor death may precede that of retinal pigment epithelium or loss of choroidal vascularization

Figure 3. AAV2-SPLTH inhibits fluorescence leakage

(A) Representative pictures of FFA in different groups after different treatments. (B) The quantitative statistical plot of (A) by scoring the fluorescence leakage in each eye. Data are presented as mean ± SD ($n = 6$). (C) Representative images of H&E staining after different treatments. (D) Statistics of the number of cells in the ONL layer in (B). Data are presented as mean ± SD ($n = 6$). One-way ANOVA method was applied for statistical analysis. $^{*}p < 0.05$, $^{**}p < 0.01$, $^{***}p < 0.001$, $^{****}p < 0.0001$, ns, not significant.

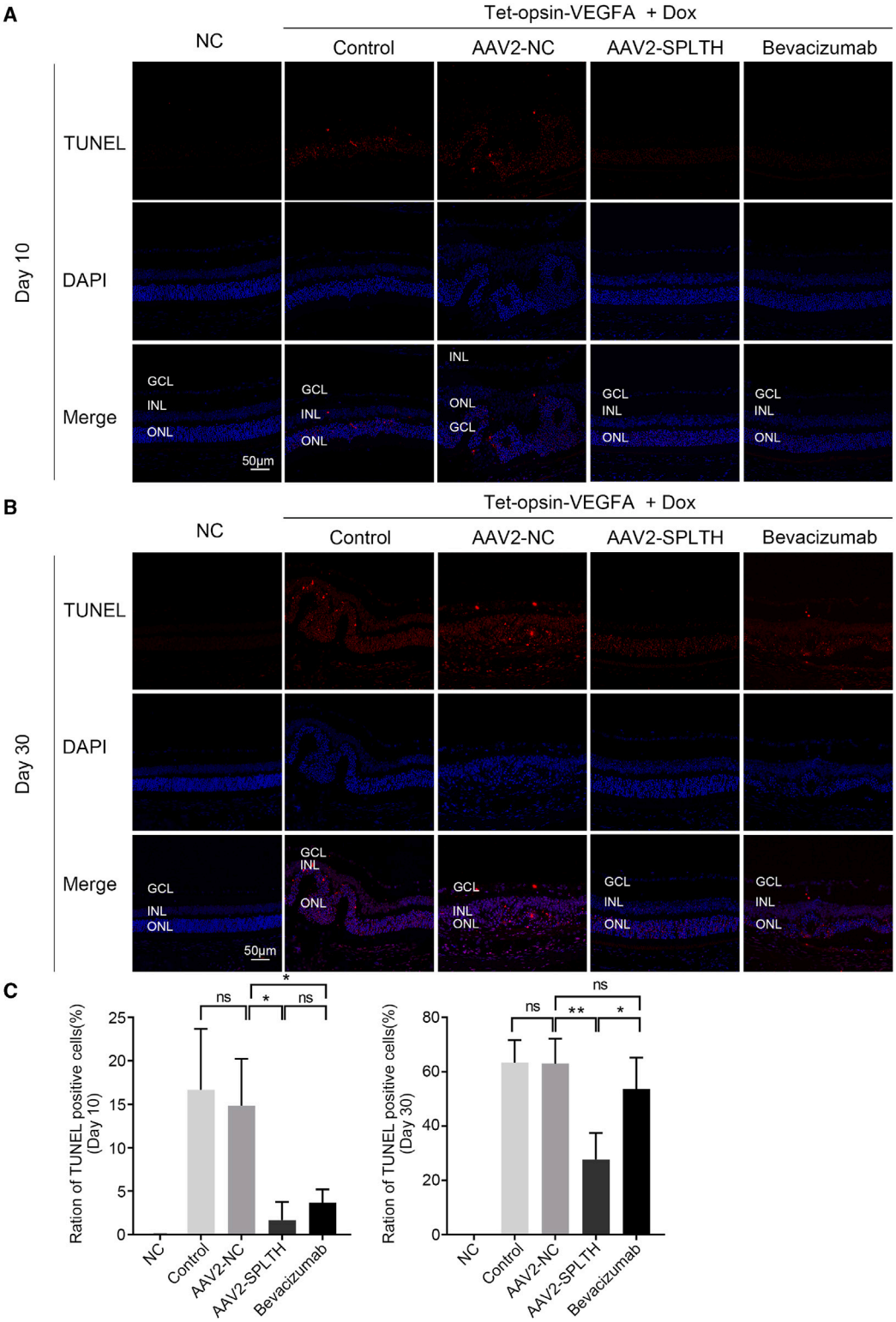

(legend on next page)

in AMD disease progression.[45] In clinical treatment, long-term anti-VEGF treatment often does not improve patient vision.[46] To explore the reasons for the insufficient rescue of photoreceptor cells by AAV2-SPLTH, we compared the proteomic characteristics of eye tissue samples between the NC, control, and AAV2-SPLTH-treated *Tet-opsin-VEGFA* mice. The most significantly downregulated protein in the control group was Rho, a protein specific to rod photoreceptors that is critical for vision in dark environments.[47] The downregulation of Rho partly reveals why VEGF-induced retinal vasculopathy seriously affects visual function. The significantly upregulated proteins Chil3, S100A9, and LCN2 in the control group were significantly downregulated in the AAV2-SPLTH group, indicating that the anti-VEGF treatment rescued the changes in these proteins, which may serve as markers for evaluating the therapeutic effect. This is consistent with the proteomic results of aqueous humor samples after clinical anti-VEGF treatment.[48] KEGG enrichment analysis revealed that the proteins that were not effectively improved by AAV2-SPLTH were mainly involved in the phototransduction signaling pathway, which corresponds to the reduction in photoreceptor cell number. In addition, the significantly enriched biosynthetic pathways of ubiquinone and other quinones are central to mitochondrial electron transfer and oxidative phosphorylation processes.[49] Oxidative phosphorylation and dysregulation of the tricarboxylic acid pathway have been reported to retard cell anabolism under hypoxic conditions, which occurs before rod cell degeneration, suggesting that changes in metabolic status may be key drivers of photoreceptor cell activity and function in fundus-angiogenesis-related diseases.[50] In the AAV2-SPLTH group, the expression of the phototransduction pathway recovery protein recoverin decreased most significantly, which can be used as an effector protein indicator of disease progression. Recoverin, a calcium-binding protein, regulates the phototransduction cascade in cone and rod cells under dark or dim background light; however, its effect on photoreceptor cell survival, morphology, and function is unclear.[51,52] The ERG reflects the action potential generated by different cells of the retina stimulated by a brief flash of light, which corresponds to retinal function. A-waves are mainly produced by photoreceptor cells, whereas B-waves are mainly produced by Müller and bipolar cells. Our ERG analysis showed that the amplitude of the A-wave remained significantly reduced in the AAV2-SPLTH-treated *Tet-opsin-VEGFA* mouse model, reflecting the reduction in photoreceptor cell numbers. These results suggest that anti-VEGF monotherapy failed to restore visual function. In fact, many patients suffer from incomplete response to anti-VEGF therapy, including suboptimal vision recovery.[4,53] Our research is consistent with the fact that anti-VEGF monotherapy does not significantly improve visual function.

In the future, we will consider the development of dual- or multi-target AAV-based drugs for sustained and comprehensive treatment of RNV. We will also explore the potential of integrating drugs with enhanced transgene expression into anti-VEGF treatment strategies.[54] Our study elucidates the pathogenesis and provides new insights into the treatment and development of drugs against RNV.

MATERIALS AND METHODS

Cell culture

HEK293T cells were purchased from Procell Life Science & Technology (Wuhan, China) and cultured in DMEM (Gibco, San Diego, CA, USA) supplemented with 10% fetal bovine serum (FBS) (DairyTech, Strathalbyn, SA, Australia). HUVECs were purchased from ScienCell Research Laboratories (San Diego, CA, USA) and cultured in endothelial cell medium (ECM) supplemented with 5% FBS, 1% endothelial cell growth supplement, and 1% penicillin-streptomycin solution (ScienCell). Human retinal pigment epithelial cells (ARPE19s) were purchased from Procell Life Science & Technology and cultured in DMEM/F-12 (Gibco) supplemented with 10% FBS. All cells were cultured at 37°C and 5% CO_2.

Tet-opsin-VEGFA mouse model and treatment

Tet-opsin-VEGFA mice were purchased from the Shanghai Model Organisms Center. This study was approved by the Laboratory Animal Welfare and Ethics Committee of China Medical University (approval no. CMU2021552). All animal testing procedures were performed in accordance with the Society for Research in Vision and Ophthalmology guidelines.

Tet-opsin-VEGFA double-transgenic mice aged 6–8 weeks were randomly divided into 4 groups. The eyes of each mouse were given the same treatment: intravitreal injection of 2 μL AAV2-NC or 3×10^9 GC AAV2-SPLTH. After 2 weeks of injection, 2 mg/mL doxycycline (MCE, HY-N0565B) was given by means of drinking water for induction, as previously described.[21] The day before doxycycline induction, both eyes of positive control mice were injected with 2 μL bevacizumab at a concentration of 25 mg/mL. In addition, mice in the control group were only given doxycycline induction. Meanwhile, wild-type mice were used as a NC group without any treatment. The effect of AAV2-SPLTH on vascular pathology was evaluated at 10 and 30 days after doxycycline induction. The flow chart of the experiment time is shown in Figure S3. Three mice in each group and six eyes were included in the statistical results.

Intravitreal injection

First, the mice were anesthetized with 1% pentobarbital sodium (50 mg/kg), and compound tropicamide drops were administered on the corneal surface. Next, 2 μL solution was injected into the vitreous. The 33G beveled needle affixed to a Hamilton syringe (2.5 μL; Hamilton, Reno, NV, USA) was used to puncture into the vitreous cavity medially at the corneoscleral rim and then slowly pushed in

Figure 4. AAV2-SPLTH could not completely save photoreceptor cell layer death

(A) TUNEL assay determined the effect of AAV2-SPLTH on cell apoptosis after 10 days of doxycycline (Dox) induction. (B) TUNEL assay determined the effect of AAV2-SPLTH on cell apoptosis after 30 days of Dox induction. (C) Analysis of the TUNEL-positive cell rates. Data are presented as mean ± SD ($n = 6$). One-way ANOVA method was applied for statistical analysis, and data are mean ± standard error. $^*p < 0.05$, $^{**}p < 0.01$, $^{***}p < 0.001$, ns, not significant.

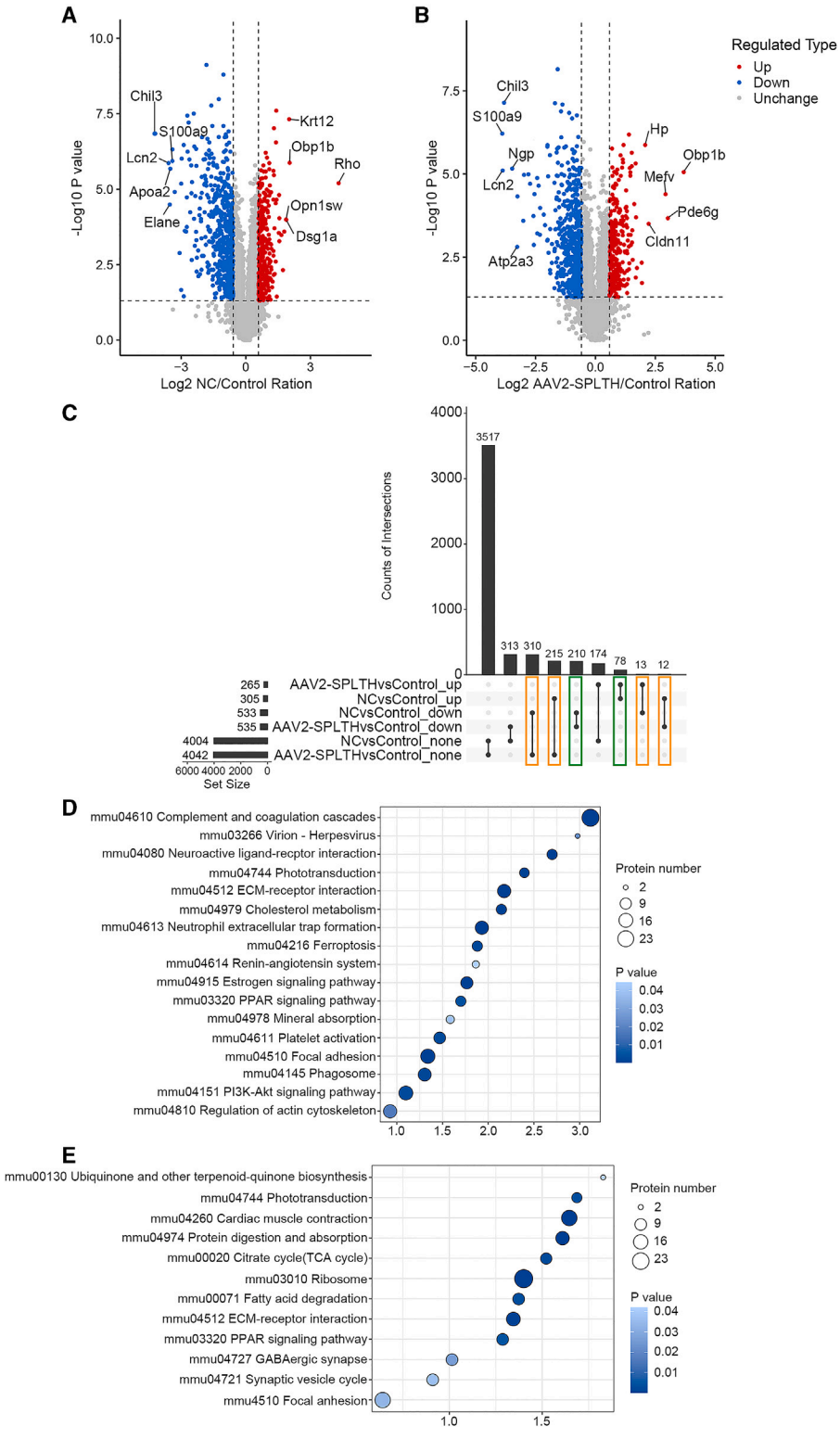

(legend on next page)

under a stereomicroscope to avoid lens injury. Immediately after the syringe was withdrawn, levofloxacin hydrochloride gel was applied to the inlet port to prevent drug leakage and infection after the operation.

Protein extraction

At 10 or 30 days after induction, the eyes of *Tet-opsin-VEGFA* mice were removed, quickly frozen in liquid nitrogen, and fully ground to a powder. The volume of NP40 lysate (N8032, Solarbio, Beijing, China) was added approximately five times, and PMSF (P0100, Solarbio) was added at a 1:100 ratio to extract the total proteins by ultrasonic cracking. The protein concentration was determined using a BCA protein concentration assay kit (PC0020, Solarbio).

Western blotting

The total protein sample was denatured by boiling in SDS sample buffer, divided into 10 μg portions in 12% SDS-PAGE gel, and transferred onto a PVDF membrane. The membrane was first sealed with 5% skim milk in TBST buffer for 2 h and then incubated with the primary antibody at 4°C overnight. After washing three times with TBST, the membrane was incubated at room temperature with a closed solution of secondary antibody for 2 h. The membrane was washed three times, incubated with chemiluminescent substrate SuperSignal West Pico PLUS (34577, Thermo Fisher Scientific, Waltham, MA, USA) according to the manufacturer's protocol, and prepared for testing. The following antibodies and concentrations were used: rabbit anti-Recoverin (10073-1, Proteintech, 1:1,000), rabbit anti-Rho (D4B9B, CST, 1:1,000), rabbit anti-actin (20536-1, Proteintech, 1:5,000), and HRP polyclonal goat anti-rabbit IgG (SA00001-2, Proteintech, 1:10,000).

ELISA

Anti-VEGF-binding ability of antibodies was analyzed by ELISA. 1 mg/mL human VEGF (Z02689, Genscript, Nanjing, China) was coated in an immunotransparent standard plate (468667, Thermo Scientific) and incubated overnight at 4°C. The plates were closed in 2% BSA for 1 h at room temperature. The test sample and bevacizumab standard were placed into the well and incubated at 37°C for 1.5 h. After washing 5 times, each well was incubated with 100 μL anti-bevacizumab antibody at 37°C for 2 h. After washing 5 times, each well was incubated with 100 μL HRP anti-rabbit IgG1 at 37°C for 1 h. After washing the plates seven times, 100 μL TMB substrate (T0440, Sigma, St. Louis, MO, USA) was added to each well and incubated at 37°C under dark conditions for 15 min. Then, 50 μL stop solution ($2NH_2SO_4$) was added to each well, and the plate was determined at 450 nm.

Cell proliferation

HUVECs were harvested at the logarithmic growth stage, digested with 0.25% trypsin, and resuspended in ECM containing FBS. The cell suspension density was adjusted to 1×10^5 cells/mL; 100 μL was added per well in 96-well plates and cultured in 5% CO_2 at 37°C for 24 h. On the second day, the medium was removed, ECM without FBS was added, and the cells were cultured under starved conditions for 12–24 h. The corresponding stimulation was applied. Three parallel holes were set in each group and cultured in an incubator for 48 h. Next, 10 μL MTS detection reagent (G3582, Promega, Madison, WI, USA) was added to each hole, and the plates were further incubated for 2 h. The optical density (OD) values of each well were measured at 450 nm using an enzyme-labeled instrument. Cell survival rates were calculated according to the following formula: cell survival rate (%) = [(experimental OD value – blank OD value)/(control OD value – blank OD value)] × 100%.

Cell migration

HUVECs at the logarithmic growth stage were harvested, digested using pancreatic enzymes, and resuspended in ECM containing FBS; the cell suspension density was adjusted to 5×10^5 cells/mL. The cells were inoculated onto 6-well plates at a density of 2 mL per well and cultured in an incubator for 24 h. At a cell density of 70%–80% determined under a microscope on the second day, the original medium was discarded, and serum-free medium containing AAV2-SPLTH (MOI = 1×10^6) or an equal volume of AAV2-NC was added. On the second day, 1×10^6 HUVECs were inoculated onto a 6-well plate per well. Marks were made on the bottom of the outer side of the well plate in advance, at least two straight lines were passed through each hole, and the cells were cultured in an incubator. After 72 h of viral infection, the medium was collected with a 5 mL centrifuge tube and centrifuged at 5,000 rpm for 5 min; the upper cell-free medium was collected for use. The colonies on the 6-well plate were scratched using a sterile 20 μL pipette tip and then subjected to the different treatments. The cells were incubated for 0–24 h, and the scratch healing rate was determined using cell images obtained with an inverted fluorescence microscope at 0, 10, and 24 h. ImageJ software (NIH v.1.53e) was used to measure the scratch area, and the healing rate was calculated according to the following formula: scratch healing rate (%) = (0 h scratch area – 10 h scratch area)/0 h scratch area × 100%.

Tube formation

At a cell density of 70%–80%, the cells were infected with an AAV, and a cell suspension (2×10^4 cells/mL) was prepared 48 h after infection. The pre-cooled 96-well cell culture plates were placed on ice,

Figure 5. Proteomic analysis of AAV2-SPLTH–mediated antiangiogenic effects in *Tet-opsin-VEGFA* mice

(A) Volcano plot shows proteins that differ significantly between untread and Dox groups based on fold change and *p* value. In particular, blue (fold change < 0.67; $p < 0.05$) or red (fold change >1.5; $p < 0.05$) dots indicate the presence of significantly downregulated or upregulated metabolites, respectively. Gray dots were non-significantly different compounds. $n = 3$. (B) Volcano plot shows protein that differ significantly between Dox and AAV2-SPLTH groups. (C) UpSet Venn diagram showed differential protein intersection analysis in untreated group, Dox group, and AAV2-SPLTH group. The green box is the saved protein set of AAV2-SPLTH, and the orange box is the unsaved protein set of AAV2-SPLTH. (D) KEGG enrichment analysis of AAV2-SPLTH salvage protein collection. (E) KEGG enrichment analysis of AAV2-SPLTH unsalvaged protein collection.

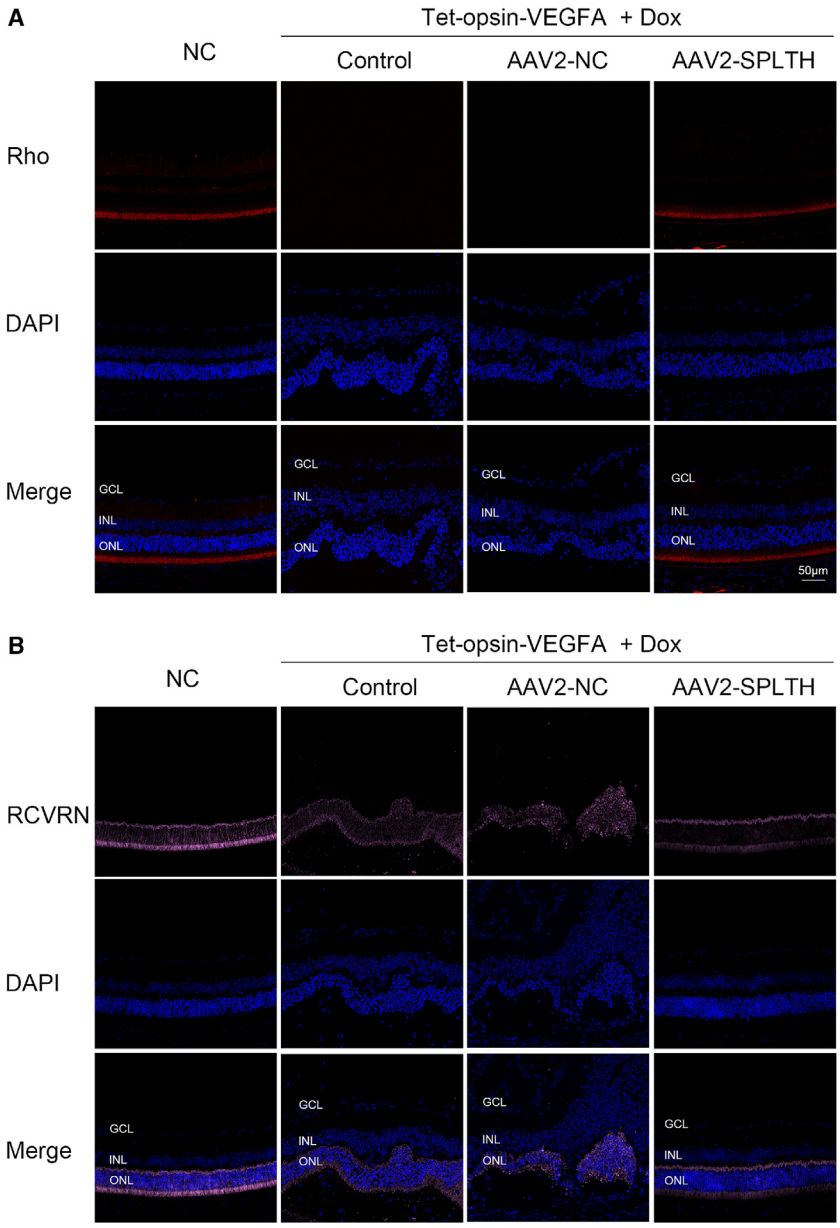

Figure 6. Immunofluorescence staining in the eyes of *Tet-opsin-VEGFA* mice

(A) Immunofluorescence staining of RCVRN on retina sections. (B) Immunofluorescence staining of RCVRN on retina sections. Scale bars: 50 μm.

50 μL matrix glue was added to each hole, and the plates were placed in an incubator at 37°C for 30 min. The prepared cell suspension was inoculated on a matrix-coated plate with a volume of 100 μL per well and cultured for 0, 3, and 6 h. The cells were observed and photographed under a 10× magnification using the inverted microscope. ImageJ software was used to measure the tube formation rate. The experiment was repeated three times, and the mean was used in the quantitative analysis.

RT-qPCR

After the mice were euthanized, their eyes were removed, quickly frozen in liquid nitrogen, and crushed to a powder. Total RNA was extracted using 1 mL TRIzol (Tiangen, Beijing, China) according to the manufacturer's instructions. We used a PrimeScript RT Kit (RR037A, Takara, Kusatsu, Japan) for reverse transcription and Hieff UNICON Universal Blue qPCR SYBR Green Master Mix (11184ES08, Yisheng, Shanghai, China) for qPCR under the following thermal cycling procedure: pre-degradation at 95°C for 2 min, followed by 40 cycles at 95°C for 10 s and 60°C for 30 s, with dissolution curves generated using default settings. The $2^{-\Delta\Delta CT}$ method was used to calculate the relative expression of mRNA. The mRNA expression of target genes was normalized to that of *GAPDH*. The primers used for RT-qPCR are shown in Table S1.

FFA

After successful model induction, the mice were anesthetized with 1% sodium pentobarbital at 0.05 mL/10 g body weight. Each mouse was intraperitoneally injected with 0.05 mL 10% fluorescein sodium, and FFA images were obtained 5 min later using a digital fundus camera (Heidelberg Engineering, Heidelberg, Germany) according to the manufacturer's instructions. To facilitate quantitative analysis, we added scores corresponding to different disease severity levels. The FFA scoring standard was based on the Diabetic Retinopathy Severity Scale.[55]

H&E staining

Mice were euthanized, eyes were removed and frozen, and 10 μm serial sections were cut. Sections were partially post-fixed in 4% paraformaldehyde, stained with H&E staining, and examined by light microscopy to determine the presence and extent of exudative retinal detachment.

Immunofluorescence

Paraffin sections of eye tissue were taken, closed with 2% BSA, and washed in PBS, followed by incubation with rabbit anti-Recoverin and anti-Rho. After that, the slides were incubated with Cy3 fluorescent-labeled goat anti-rabbit IgG (GB21303, Servicebio, Wuhan, China) or Cy5 fluorescent-labeled goat anti-rabbit IgG (GB27303, Servicebio). After incubation, nuclei were restained with DAPI solution, and fluorescent images were collected by microscopy for analysis.

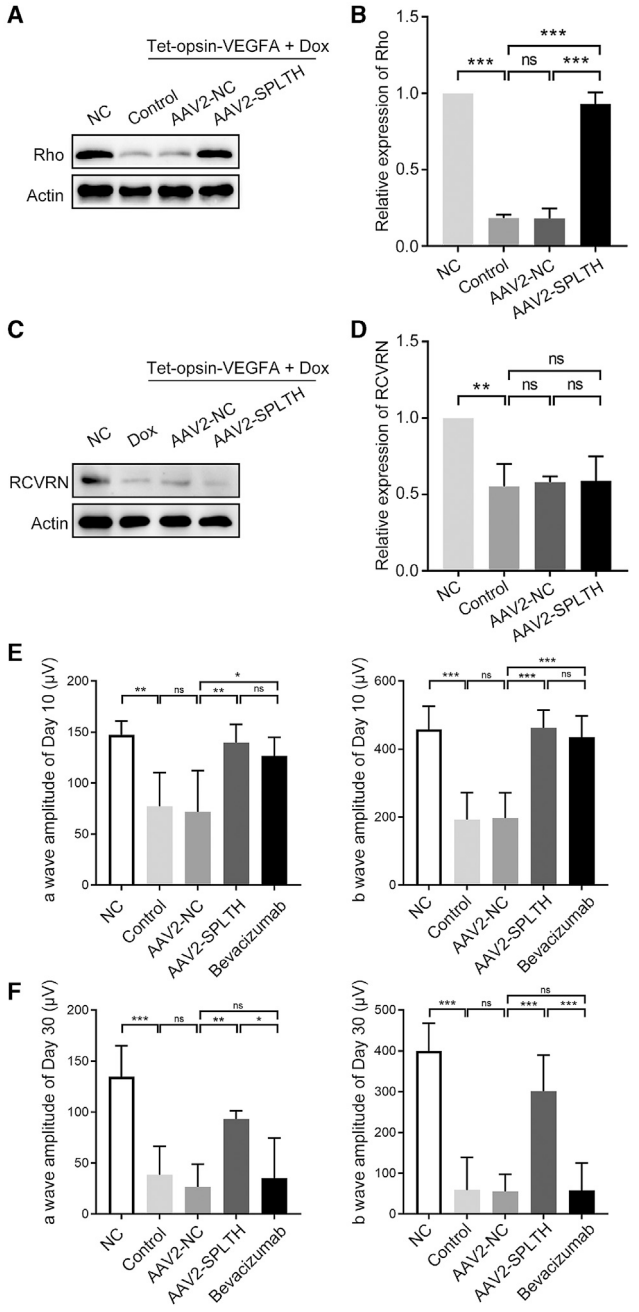

Figure 7. Evaluation of protein expression and ERG in the eyes of *Tet/opsin/VEGFA* mice

(A) Western blot analysis of the Rho expression levels (actin was used as an internal control). (B) The relative protein expression intensity of Rho. Data are presented as mean ± SD (n = 3). (C) Western blot analysis of the RCVRN expression levels (actin was used as an internal control). (D) The relative protein expression intensity of RCVRN. Data are presented as mean ± SD (n = 3). (E) Scotopic ERG showing A-wave or B-wave amplitudes at 10 days after Dox induction (n = 6). (F) Scotopic ERG showing A-wave or B-wave amplitudes at 30 days after Dox induction (n = 6). One-way ANOVA method was applied for statistical analysis, and data are mean ± SD. $^{**}p < 0.01$, $^{***}p < 0.001$, ns, not significant.

ERG

The mice were placed in a dark room overnight (at least 12 h) prior to the examination. After anesthesia, the mice were fixed on the operating table, pupil-dilating drops were added, electrodes were fitted, and the ERG was measured and recorded using a Diagnosys Celeris small-animal electrophysiologist.

Proteotranscriptome

Immediately after killing the mice, the eyeball tissue was removed, quickly frozen in liquid nitrogen, and fully ground to a powder. The volume of cracking buffer (8 M urea, 1% protease inhibitor) was added to each group of samples 5 times, the protein was extracted, and the protein concentration was determined.

The same amount of protein was taken from each group for enzymolysis, and the volume was adjusted to be consistent with the lysate. The volume of pre-cooled acetone was added 1 time, swirled and mixed well, and then the volume of pre-cooled acetone was added 4 times and precipitated at −20°C for 2 h. The collected samples were centrifuged at 4500g for 5 minutes. Then, the supernatant in the test tube was discarded and washed twice with pre-cooled acetone. After drying and precipitation, TEAB with a final concentration of 200 mM was added, the precipitation was dispersed by ultrasound, and trypsin was added at a ratio of 1:50. The final concentration of dithiothreitol was 5 mM and reduced at 56°C for 30 min. Then, iodoacetamide was added to make its final concentration 11 mM and incubated at room temperature for 15 min away from light.

The peptides were dissolved by liquid chromatography mobile phase A and separated by a NanoElute ultra-high performance liquid phase system.

The detected proteins were annotated and classified into Gene Ontology (GO) using Eggnog-Mapper software (v.2.1.6), which was based on the EggNOG database. The GO IDs in the protein annotation results were extracted and then functionally classified according to cell components, molecular functions, and biological processes. We annotated the protein pathways based on the KEGG pathway database, blasted the identified proteins, and selected the comparison results with the highest scores for annotation.

Fisher's exact test was used to enrich the GO and KEGG pathways of differentially expressed proteins, and $p < 0.05$ was considered statistically significant.

Data analysis

All data were analyzed using GraphPad Prism software (v.8.0; GraphPad Software, San Diego, CA, USA). For two-way comparisons of data following a Gaussian distribution, data were analyzed using an unpaired two-tailed t test. Statistically significant differences between two or more groups were tested using a one-way ANOVA with a post hoc Scheffe test. Statistical significance was set at $p < 0.05$. All data are expressed as the mean ± standard deviation.

DATA AND CODE AVAILABILITY

The data used and/or analyzed during the current study are available from the corresponding author upon reasonable request.

SUPPLEMENTAL INFORMATION

Supplemental information can be found online at https://doi.org/10.1016/j.omtn.2024.102176.

ACKNOWLEDGMENTS

This work is supported by the National Natural Science Foundation of China (no. 82070826).

AUTHOR CONTRIBUTIONS

Conceptualization, visualization, and project administration, X.X., N.H., R.F., Y.L., and G.L.; investigation, X.X., N.H., Y.L., and G.L.; methodology, data curation, and formal analysis, X.X., N.H., F.Z., R.F., Q.G.; resources and software, F.Z., X.H., Y.L., and G.L.; writing – original draft, X.X., R.F., Y.L., and G.L.; writing – review & editing, X.X., R.F., Y.L. and G.L.; supervision, Y.L. and G.L.; funding acquisition, Y.L. and G.L.

DECLARATION OF INTERESTS

The authors declare no competing interests.

REFERENCES

1. Campochiaro, P.A. (2015). Molecular pathogenesis of retinal and choroidal vascular diseases. Prog. Retin. Eye Res. *49*, 67–81.
2. Fleckenstein, M., Keenan, T.D.L., Guymer, R.H., Chakravarthy, U., Schmitz-Valckenberg, S., Klaver, C.C., Wong, W.T., and Chew, E.Y. (2021). Age-related macular degeneration. Nat. Rev. Dis. Prim. *7*, 31.
3. Wong, T.Y., Cheung, C.M.G., Larsen, M., Sharma, S., and Simó, R. (2016). Diabetic retinopathy. Nat. Rev. Dis. Prim. *2*, 16012.
4. Mettu, P.S., Allingham, M.J., and Cousins, S.W. (2021). Incomplete response to Anti-VEGF therapy in neovascular AMD: Exploring disease mechanisms and therapeutic opportunities. Prog. Retin. Eye Res. *82*, 100906.
5. Campochiaro, P.A. (2013). Ocular neovascularization. J. Mol. Med. *91*, 311–321.
6. Miller, J.W., Le Couter, J., Strauss, E.C., and Ferrara, N. (2013). Vascular endothelial growth factor a in intraocular vascular disease. Ophthalmology *120*, 106–114.
7. Toutounchian, S., Ahmadbeigi, N., and Mansouri, V. (2022). Retinal and Choroidal Neovascularization Antivascular Endothelial Growth Factor Treatments: The Role of Gene Therapy. J. Ocul. Pharmacol. Therapeut. *38*, 529–548.
8. ElSheikh, R.H., Chauhan, M.Z., and Sallam, A.B. (2022). Current and Novel Therapeutic Approaches for Treatment of Neovascular Age-Related Macular Degeneration. Biomolecules *12*, 1629.
9. Xiao, H., Zhao, X., Li, S., Sun, L., Xin, W., Wang, Z., Zhang, A., Zhang, J., and Ding, X. (2021). Risk factors for subretinal fibrosis after anti-VEGF treatment of myopic choroidal neovascularisation. Br. J. Ophthalmol. *105*, 103–108.
10. Eng, V.A., Rayess, N., Nguyen, H.V., and Leng, T. (2020). Complete RPE and outer retinal atrophy in patients receiving anti-VEGF treatment for neovascular age-related macular degeneration. PLoS One *15*, e0232353.
11. Su, J., She, K., Song, L., Jin, X., Li, R., Zhao, Q., Xiao, J., Chen, D., Cheng, H., Lu, F., et al. (2023). In vivo base editing rescues photoreceptors in a mouse model of retinitis pigmentosa. Mol. Ther. Nucleic Acids *31*, 596–609.
12. Colella, P., and Auricchio, A. (2010). AAV-mediated gene supply for treatment of degenerative and neovascular retinal diseases. Curr. Gene Ther. *10*, 371–380.
13. Tian, X., Zheng, Q., Xie, J., Zhou, Q., Liang, L., Xu, G., Chen, H., Ling, C., and Lu, D. (2023). Improved gene therapy for MFRP deficiency-mediated retinal degeneration by knocking down endogenous bicistronic Mfrp and Ctrp5 transcript. Mol. Ther. Nucleic Acids *32*, 843–856.
14. Khanani, A.M., Thomas, M.J., Aziz, A.A., Weng, C.Y., Danzig, C.J., Yiu, G., Kiss, S., Waheed, N.K., and Kaiser, P.K. (2022). Review of gene therapies for age-related macular degeneration. Eye *36*, 303–311.
15. Wykoff, C.C., Abreu, F., Adamis, A.P., Basu, K., Eichenbaum, D.A., Haskova, Z., Lin, H., Loewenstein, A., Mohan, S., Pearce, I.A., et al. (2022). Efficacy, durability, and safety of intravitreal faricimab with extended dosing up to every 16 weeks in patients with diabetic macular oedema (YOSEMITE and RHINE): two randomised, double-masked, phase 3 trials. Lancet *399*, 741–755.
16. Shtivelman, E., Sussman, J., and Stokoe, D. (2002). A role for PI 3-kinase and PKB activity in the G2/M phase of the cell cycle. Curr. Biol. *12*, 919–924.
17. Kiss, S., Oresic Bender, K., Grishanin, R.N., Hanna, K.M., Nieves, J.D., Sharma, P., Nguyen, A.T., Rosario, R.J., Greengard, J.S., Gelfman, C.M., and Gasmi, M. (2021). Long-Term Safety Evaluation of Continuous Intraocular Delivery of Aflibercept by the Intravitreal Gene Therapy Candidate ADVM-022 in Nonhuman Primates. Transl. Vis. Sci. Technol. *10*, 34.
18. van Dijk, H.W., Verbraak, F.D., Stehouwer, M., Kok, P.H.B., Garvin, M.K., Sonka, M., DeVries, J.H., Schlingemann, R.O., and Abràmoff, M.D. (2011). Association of visual function and ganglion cell layer thickness in patients with diabetes mellitus type 1 and no or minimal diabetic retinopathy. Vis. Res. *51*, 224–228.
19. Himasa, F.I., Singhal, M., Ojha, A., and Kumar, B. (2022). Prospective for Diagnosis and Treatment of Diabetic Retinopathy. Curr. Pharmaceut. Des. *28*, 560–569.
20. Altmann, C., and Schmidt, M.H.H. (2018). The Role of Microglia in Diabetic Retinopathy: Inflammation, Microvasculature Defects and Neurodegeneration. Int. J. Mol. Sci. *19*, 110.
21. Ohno-Matsui, K., Hirose, A., Yamamoto, S., Saikia, J., Okamoto, N., Gehlbach, P., Duh, E.J., Hackett, S., Chang, M., Bok, D., et al. (2002). Inducible expression of vascular endothelial growth factor in adult mice causes severe proliferative retinopathy and retinal detachment. Am. J. Pathol. *160*, 711–719.
22. Streisinger, G., Walker, C., Dower, N., Knauber, D., and Singer, F. (1981). Production of clones of homozygous diploid zebra fish (Brachydanio rerio). Nature *291*, 293–296.
23. Meyer, N.L., and Chapman, M.S. (2022). Adeno-associated virus (AAV) cell entry: structural insights. Trends Microbiol. *30*, 432–451.
24. Hussain, R.M., Shaukat, B.A., Ciulla, L.M., Berrocal, A.M., and Sridhar, J. (2021). Vascular Endothelial Growth Factor Antagonists: Promising Players in the Treatment of Neovascular Age-Related Macular Degeneration. Drug Des. Dev. Ther. *15*, 2653–2665.
25. Terasaki, H., Sakamoto, T., Shirasawa, M., Yoshihara, N., Otsuka, H., Sonoda, S., Hisatomi, T., and Ishibashi, T. (2015). Penetration of bevacizumab and ranibizumab through retinal pigment epithelial layer in vitro. Retina *35*, 1007–1015.
26. Diabetic Retinopathy Clinical Research, N., Wells, J.A., Glassman, A.R., Ayala, A.R., Jampol, L.M., Aiello, L.P., Antoszyk, A.N., Arnold-Bush, B., Baker, C.W., Bressler, N.M., et al. (2015). Aflibercept, bevacizumab, or ranibizumab for diabetic macular edema. N. Engl. J. Med. *372*, 1193–1203.
27. Avery, R.L., Castellarin, A.A., Steinle, N.C., Dhoot, D.S., Pieramici, D.J., See, R., Couvillion, S., Nasir, M.A., Rabena, M.D., Maia, M., et al. (2017). Systemic Pharmacokinetics and Pharmacodynamics of Intravitreal Aflibercept, Bevacizumab, and Ranibizumab. Retina *37*, 1847–1858.
28. Durairaj, C. (2017). Ocular Pharmacokinetics. Handb. Exp. Pharmacol. *242*, 31–55.
29. Igarashi, T., Miyake, K., Masuda, I., Takahashi, H., and Shimada, T. (2010). Adeno-associated vector (type 8)-mediated expression of soluble Flt-1 efficiently inhibits neovascularization in a murine choroidal neovascularization model. Hum. Gene Ther. *21*, 631–637.
30. Krohne, T.U., Eter, N., Holz, F.G., and Meyer, C.H. (2008). Intraocular pharmacokinetics of bevacizumab after a single intravitreal injection in humans. Am. J. Ophthalmol. *146*, 508–512.
31. Krohne, T.U., Liu, Z., Holz, F.G., and Meyer, C.H. (2012). Intraocular pharmacokinetics of ranibizumab following a single intravitreal injection in humans. Am. J. Ophthalmol. *154*, 682–686.e2.

32. Do, D.V., Rhoades, W., and Nguyen, Q.D. (2020). Pharmacokinetic Study of Intravitreal Aflibercept in Humans with Neovascular Age-Related Macular Degeneration. Retina *40*, 643–647.

33. Li, C., and Samulski, R.J. (2020). Engineering adeno-associated virus vectors for gene therapy. Nat. Rev. Genet. *21*, 255–272.

34. You, M., Yang, Y., Zhong, C., Chen, F., Wang, X., Jia, T., Chen, Y., Zhou, B., Mi, Q., Zhao, Q., et al. (2018). Efficient mAb production in CHO cells with optimized signal peptide, codon, and UTR. Appl. Microbiol. Biotechnol. *102*, 5953–5964.

35. Gupta, K., Parasnis, M., Jain, R., and Dandekar, P. (2019). Vector-related stratagems for enhanced monoclonal antibody production in mammalian cells. Biotechnol. Adv. *37*, 107415.

36. Chatziralli, I.P., and Sergentanis, T.N. (2017). Ocular gene therapy for neovascular AMD: a new era? Lancet (London, England) *390*, 2139–2140.

37. Zeng, H., Horie, K., Madisen, L., Pavlova, M.N., Gragerova, G., Rohde, A.D., Schimpf, B.A., Liang, Y., Ojala, E., Kramer, F., et al. (2008). An inducible and reversible mouse genetic rescue system. PLoS Genet. *4*, e1000069.

38. Okamoto, N., Tobe, T., Hackett, S.F., Ozaki, H., Vinores, M.A., LaRochelle, W., Zack, D.J., and Campochiaro, P.A. (1997). Transgenic mice with increased expression of vascular endothelial growth factor in the retina: a new model of intraretinal and subretinal neovascularization. Am. J. Pathol. *151*, 281–291.

39. Del Amo, E.M., Rimpelä, A.K., Heikkinen, E., Kari, O.K., Ramsay, E., Lajunen, T., Schmitt, M., Pelkonen, L., Bhattacharya, M., Richardson, D., et al. (2017). Pharmacokinetic aspects of retinal drug delivery. Prog. Retin. Eye Res. *57*, 134–185.

40. Grishanin, R., Vuillemenot, B., Sharma, P., Keravala, A., Greengard, J., Gelfman, C., Blumenkrantz, M., Lawrence, M., Hu, W., Kiss, S., and Gasmi, M. (2019). Preclinical Evaluation of ADVM-022, a Novel Gene Therapy Approach to Treating Wet Age-Related Macular Degeneration. Mol. Ther. *27*, 118–129.

41. Campbell, M., and Doyle, S.L. (2019). Current perspectives on established and novel therapies for pathological neovascularization in retinal disease. Biochem. Pharmacol. *164*, 321–325.

42. Ehlken, C., Jungmann, S., Böhringer, D., Agostini, H.T., Junker, B., and Pielen, A. (2014). Switch of anti-VEGF agents is an option for nonresponders in the treatment of AMD. Eye *28*, 538–545.

43. Quaggin, S.E. (2012). Turning a blind eye to anti-VEGF toxicities. J. Clin. Invest. *122*, 3849–3851.

44. Saint-Geniez, M., Maharaj, A.S.R., Walshe, T.E., Tucker, B.A., Sekiyama, E., Kurihara, T., Darland, D.C., Young, M.J., and D'Amore, P.A. (2008). Endogenous VEGF is required for visual function: evidence for a survival role on müller cells and photoreceptors. PLoS One *3*, e3554.

45. Zekavat, S.M., Sekimitsu, S., Ye, Y., Raghu, V., Zhao, H., Elze, T., Segrè, A.V., Wiggs, J.L., Natarajan, P., Del Priore, L., et al. (2022). Photoreceptor Layer Thinning Is an Early Biomarker for Age-Related Macular Degeneration: Epidemiologic and Genetic Evidence from UK Biobank OCT Data. Ophthalmology *129*, 694–707.

46. Lamb, T.D. (2020). Evolution of the genes mediating phototransduction in rod and cone photoreceptors. Prog. Retin. Eye Res. *76*, 100823.

47. Liu, J., Liu, M.Y., Nguyen, J.B., Bhagat, A., Mooney, V., and Yan, E.C.Y. (2011). Thermal properties of rhodopsin: insight into the molecular mechanism of dim-light vision. J. Biol. Chem. *286*, 27622–27629.

48. Tsai, C.Y., Chen, C.T., Wu, H.H., Liao, C.C., Hua, K., Hsu, C.H., and Chen, C.F. (2022). Proteomic Profiling of Aqueous Humor Exosomes from Age-related Macular Degeneration Patients. Int. J. Med. Sci. *19*, 893–900.

49. Ikunishi, R., Otani, R., Masuya, T., Shinzawa-Itoh, K., Shiba, T., Murai, M., and Miyoshi, H. (2023). Respiratory complex I in mitochondrial membrane catalyzes oversized ubiquinones. J. Biol. Chem. *299*, 105001.

50. Todorova, V., Stauffacher, M.F., Ravotto, L., Nötzli, S., Karademir, D., Ebner, L.J.A., Imsand, C., Merolla, L., Hauck, S.M., Samardzija, M., et al. (2023). Deficits in mitochondrial TCA cycle and OXPHOS precede rod photoreceptor degeneration during chronic HIF activation. Mol. Neurodegener. *18*, 15.

51. Sampath, A.P., Strissel, K.J., Elias, R., Arshavsky, V.Y., McGinnis, J.F., Chen, J., Kawamura, S., Rieke, F., and Hurley, J.B. (2005). Recoverin improves rod-mediated vision by enhancing signal transmission in the mouse retina. Neuron *46*, 413–420.

52. Morshedian, A., Woodruff, M.L., and Fain, G.L. (2018). Role of recoverin in rod photoreceptor light adaptation. J. Physiol. *596*, 1513–1526.

53. Sarkar, A., Jayesh Sodha, S., Junnuthula, V., Kolimi, P., and Dyawanapelly, S. (2022). Novel and investigational therapies for wet and dry age-related macular degeneration. Drug Discov. Today *27*, 2322–2332.

54. Xie, Y.L., Wang, J.Y., He, Y., Yu, X.M., Zheng, Q.Y., Ling, C., Feng, X.L., and Zhu, L.Q. (2023). The use of melittin to enhance transgene expression mediated by recombinant adeno-associated virus serotype 2 vectors both in vitro and in vivo. J. Integr. Med. *21*, 106–115.

55. Wilkinson, C.P., Ferris, F.L., 3rd, Klein, R.E., Lee, P.P., Agardh, C.D., Davis, M., Dills, D., Kampik, A., Pararajasegaram, R., and Verdaguer, J.T.; Global Diabetic Retinopathy Project Group (2003). Proposed international clinical diabetic retinopathy and diabetic macular edema disease severity scales. Ophthalmology *110*, 1677–1682.